Quantum Error Correction: Mathematical Foundations and Analysis

Jithin Kollapudi, Krunal Vaghela, Yaswanth Ram Kumar
Department of Electrical Engineering
Indian Institute of Technology Bombay
Mumbai 400076, India

***Abstract*—This paper presents our comprehensive mathematical analysis of fundamental quantum error correction (QEC) concepts, establishing the theoretical foundation for fault-tolerant quantum computation. We develop detailed mathematical treatments of quantum error models, including coherent systematic errors and environmental decoherence, and analyze their impact on quantum algorithms. Our work provides rigorous derivations of basic error correction codes (3-qubit and 9-qubit codes), error detection schemes, and the stabilizer formalism. We establish the mathematical framework for understanding how continuous quantum noise processes can be effectively corrected through discrete error models.**

***Index Terms*—Quantum Error Correction, Stabilizer Codes, Quantum Noise Models**

1. Introduction

Quantum error correction represents one of the most vital theoretical foundations enabling the development of fault-tolerant quantum computation. The inherent fragility of coherent quantum systems presents a fundamental obstacle to building large-scale quantum computers, as quantum states are susceptible to decoherence, control errors, and environmental interactions. The mathematical framework of quantum error correction demonstrates that active techniques can mitigate these challenges, establishing that quantum computation can be made robust against realistic noise conditions.

This paper presents our mathematical analysis of fundamental QEC concepts, focusing on establishing the theoretical foundation for error correction and the crucial process of mapping continuous quantum errors to discrete correctable forms. Our study develops comprehensive treatments of quantum error models, basic error correction codes including the 3-qubit and 9-qubit codes, error detection schemes, and the powerful stabilizer formalism. Through detailed mathematical derivations and circuit-level analysis, we establish how continuous quantum noise processes—including coherent systematic errors and environmental decoherence—can be effectively addressed through discrete error correction techniques.

The error digitization mechanism, where the continuous nature of quantum errors is collapsed into discrete syndromes through measurement, represents a cornerstone of practical quantum error correction. We develop explicit mathematical treatments of this process using coherent error analysis and density matrix formalism, demonstrating how physical error mechanisms translate to the probabilistic error models employed in QEC theory.

This foundational work establishes the necessary framework for our planned implementation of fault-tolerant quantum circuits and threshold analysis in the ongoing phase of our research. By building a solid mathematical understanding of error correction techniques, we lay the groundwork for addressing more advanced topics including fault-tolerant operations, concatenated codes, and the threshold theorem in future work.

2. Mathematical Preliminaries and Challenges

2.1. Quantum Bit Fundamentals

The mathematical description of a quantum bit resides in a two-dimensional complex Hilbert space $\mathcal{H} \cong \mathbb{C}^2$. A general qubit state is represented by:

$$|\psi\rangle = \alpha\,|0\rangle + \beta\,|1\rangle\,, \quad \alpha, \beta \in \mathbb{C} \tag{1}$$

with normalization constraint:

$$\langle\psi\rangle\,\psi = |\alpha|^2 + |\beta|^2 = 1 \tag{2}$$

The state space forms a complex projective space $\mathbb{C}P^1$, where global phases are identified:

$$|\psi\rangle \sim e^{i\phi}\,|\psi\rangle \tag{3}$$

2.2. Quantum Gates and Pauli Algebra

Quantum gates are elements of the unitary group $U(2)$ with determinant constraints for special unitaries $SU(2)$. The Pauli matrices generate the Lie algebra $\mathfrak{su}(2)$:

$$X = \begin{pmatrix} 0 & 1 \\ 1 & 0 \end{pmatrix}, \quad Y \quad = \begin{pmatrix} 0 & -i \\ i & 0 \end{pmatrix}, \quad Z = \begin{pmatrix} 1 & 0 \\ 0 & -1 \end{pmatrix} \tag{4}$$

The commutation relations define the structure constants:

$$[X, Y] = 2iZ, \quad [Y, Z] = 2iX, \quad [Z, X] = 2iY \tag{5}$$

$$\sigma_i \sigma_j = \delta_{ij} I + i\epsilon_{ijk} \sigma_k \tag{6}$$

The n-qubit Pauli group is:

$$\mathcal{P}_n = \{\pm 1, \pm i\} \otimes \{I, X, Y, Z\}^{\otimes n} \tag{7}$$

2.3. Density Matrix Formalism

The state space extends to density operators $\rho \in \mathcal{L}(\mathcal{H})$ with:

$$\rho \geq 0 \quad \text{(positive semi-definite)} \tag{8}$$

$$\text{Tr}(\rho) = 1 \tag{9}$$

$$\rho^\dagger = \rho \tag{10}$$

Pure states satisfy $\rho^2 = \rho$, while mixed states have $\rho^2 \neq \rho$. The spectral decomposition:

$$\rho = \sum_i \lambda_i \left|\psi_i\right\rangle \left\langle\psi_i\right|, \quad \lambda_i \geq 0, \quad \sum_i \lambda_i = 1 \tag{11}$$

The fidelity between states is:

$$F(\rho, \sigma) = \left(\text{Tr} \sqrt{\sqrt{\rho} \sigma \sqrt{\rho}} \right)^2 \tag{12}$$

2.4. Quantum Observables and Measurement

Observables correspond to Hermitian operators $A = A^\dagger$ with real spectrum $\sigma(A) \subset \mathbb{R}$. The spectral theorem gives:

$$A = \sum_{\lambda \in \sigma(A)} \lambda P_\lambda \tag{13}$$

where P_λ are orthogonal projectors satisfying:

$$P_\lambda P_\mu = \delta_{\lambda\mu} P_\lambda \tag{14}$$

$$\sum_\lambda P_\lambda = I \tag{15}$$

The expectation value follows:

$$\mathbb{E}_\rho[A] = \text{Tr}(A\rho) = \sum_\lambda \lambda \text{Tr}(P_\lambda \rho) \tag{16}$$

The variance is:

$$\text{Var}_\rho(A) = \text{Tr}(A^2 \rho) - (\text{Tr}(A\rho))^2 \tag{17}$$

2.5. Fundamental Challenges in Quantum Error Correction

Challenge 1: No-Cloning Theorem The impossibility of perfect quantum state copying prohibits simple redundancy strategies. Formally, there exists no unitary transformation U such that:

$$U(\left|\psi\right\rangle \otimes \left|\phi\right\rangle) = \left|\psi\right\rangle \otimes \left|\psi\right\rangle \quad \forall \left|\psi\right\rangle \tag{18}$$

This algebraic constraint prohibits linear copying of non-orthogonal states.

Challenge 2: Measurement Disturbance
The projection postulate:

$$\rho \to \frac{P_m \rho P_m}{\text{Tr}(P_m \rho)}, \quad P_m = \left|m\right\rangle \left\langle m\right| \tag{19}$$

irreversibly collapses superpositions.

Challenge 3: Continuous Error Spectrum
The error manifold:

$$\mathcal{E} = \{e^{i(\theta_x X + \theta_y Y + \theta_z Z)} : \theta_i \in \mathbb{R}\} \cong SU(2) \tag{20}$$

forms a continuous group requiring discretization.

Challenge 4: Simultaneous Error Protection
The necessary condition from the Pauli algebra:

$$[X, Z] = -2iY \neq 0 \tag{21}$$

shows non-commutativity requires joint correction strategies.

2.6. Quantum Error Correction Codes

An $[[n, k, d]]$ quantum code encodes k logical qubits into n physical qubits with distance d. The code space $\mathcal{C}$ satisfies:

$$\dim \mathcal{C} = 2^k, \quad \mathcal{C} \subset (\mathbb{C}^2)^{\otimes n} \tag{22}$$

The distance d is the minimum weight of logical operators:

$$d = \min\{\text{wt}(E) : \left\langle\psi\right| E \left|\phi\right\rangle \neq 0 \text{ for some } \left|\psi\right\rangle, \left|\phi\right\rangle \in \mathcal{C}\} \tag{23}$$

The code rate and correctable errors:

$$R = \frac{k}{n} \tag{24}$$

$$t = \left\lfloor \frac{d-1}{2} \right\rfloor \tag{25}$$

Error suppression follows:

$$p_L \approx c p^{t+1}, \quad p \ll 1 \tag{26}$$

where p is physical error rate and p_L is logical error rate.

3. Quantum Errors: Physical Origins and Mathematical Models

3.1. Classification of Quantum Errors

Quantum errors arise from two primary mechanisms: (1) coherent systematic errors from imperfect gate implementations, (2) incoherent environmental decoherence from system-environment interactions and 3) operational errors including measurement imperfections, qubit loss, initialization inaccuracies, and state leakage. We analyze each through illustrative quantum algorithms.

3.2. Modeling a Coherent Rotational Error

Let's consider an experiment designed to test gate fidelity. We repeatedly apply a gate that should perform a π rotation around the x-axis ($R_x(\pi)$ gate, i.e., an X-gate). We start with a qubit in the state $|0\rangle$.

3.3. The Ideal Gate

The ideal rotation gate, $R_x(\pi)$, is represented by the unitary matrix:

$$R_x(\pi) = e^{-i\frac{\pi}{2}\sigma_x} = \begin{pmatrix} \cos(\pi/2) & -i\sin(\pi/2) \\ -i\sin(\pi/2) & \cos(\pi/2) \end{pmatrix} = \begin{pmatrix} 0 & -i \\ -i & 0 \end{pmatrix}$$

where σ_x is the Pauli-X matrix.

3.4. The Noisy Gate

A coherent error can be modeled as a small, systematic miscalibration in the rotation angle. Instead of rotating by π, the physical gate rotates by $\pi + \epsilon$ every time, where ϵ is the small error angle. The noisy gate is therefore:

$$\tilde{R}_x(\pi) = R_x(\pi + \epsilon) \tag{27}$$

3.5. Expectation Value of the Pauli-Z Observable

To see the effect of this error, we measure the expectation value of the Pauli-Z observable, $\langle Z \rangle$, after applying our gate d times (a circuit of depth d).

Why the Pauli-Z Observable?. The Pauli-Z operator has the computational basis states $|0\rangle$ and $|1\rangle$ as its eigenstates with eigenvalues $+1$ and -1, respectively. The expectation value $\langle Z \rangle = P(0) - P(1)$ is a direct measure of the qubit's bias towards the basis states, making it an excellent metric for characterizing the final state of a computation. A value of $+1$ means the qubit is definitely in $|0\rangle$, and -1 means it is definitely in $|1\rangle$.

3.6. Ideal Case

After applying the ideal gate d times, the total rotation is $d\pi$. The final state $|\psi_f\rangle$ is:

$$|\psi_f\rangle = (R_x(\pi))^d |0\rangle = R_x(d\pi) |0\rangle = \cos(\frac{d\pi}{2}) |0\rangle - i\sin(\frac{d\pi}{2}) |1\rangle$$

The expectation value $\langle Z \rangle$ is $\langle \psi_f | Z | \psi_f \rangle$:

$$\langle Z \rangle = \cos^2(\frac{d\pi}{2}) - \sin^2(\frac{d\pi}{2}) = \cos(d\pi) = (-1)^d$$

In the ideal case, the qubit perfectly flips between $|0\rangle$ and $|1\rangle$, so $\langle Z \rangle$ alternates between $+1$ and -1.

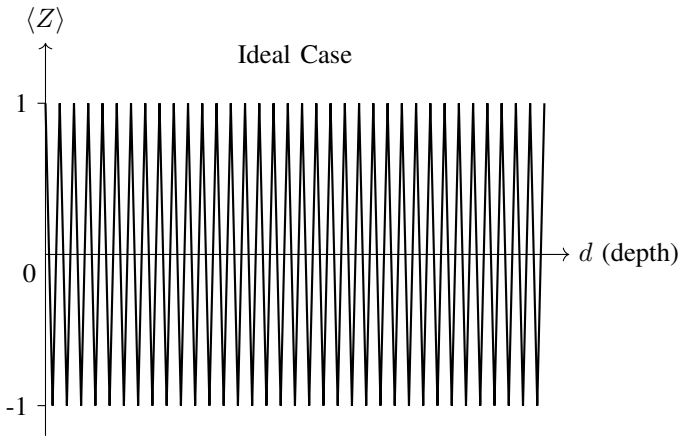

Figure 1: Expectation value $\langle Z \rangle$ vs. circuit depth for the ideal case

3.7. Noisy Case

With the coherent error, the total rotation after d gates is $d(\pi + \epsilon)$. The final state $|\tilde{\psi}_f\rangle$ is:

$$|\tilde{\psi}_f\rangle = R_x(d(\pi + \epsilon)) |0\rangle$$

The expectation value is found using the same procedure:

$$\begin{aligned} \langle \tilde{Z} \rangle &= \cos^2(\frac{d(\pi+\epsilon)}{2}) - \sin^2(\frac{d(\pi+\epsilon)}{2}) \\ &= \cos(d(\pi + \epsilon)) \\ &= \cos(d\pi)\cos(d\epsilon) - \sin(d\pi)\sin(d\epsilon) \\ &= (-1)^d \cos(d\epsilon) \end{aligned}$$

The error introduces a decaying cosine envelope, $\cos(d\epsilon)$, that modulates the ideal oscillation.

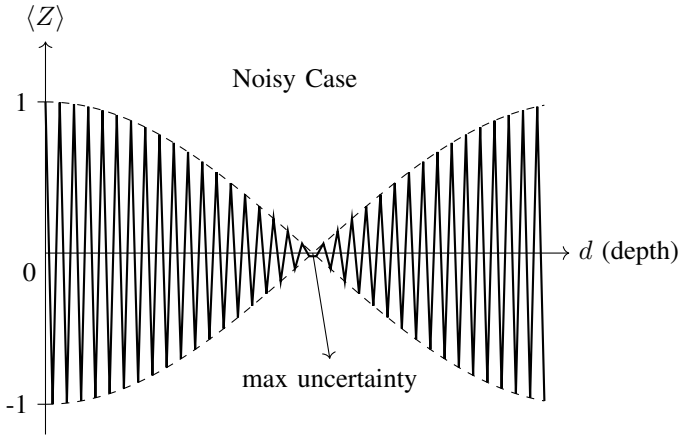

Figure 2: Expectation value $\langle Z \rangle$ vs. circuit depth for noisy case. The coherent error creates an oscillatory envelope.

3.8. Environmental Decoherence

3.8.1. System-Environment Interaction Model. Environmental decoherence arises from uncontrolled coupling to external degrees of freedom. We model this using a simple two-level environment with basis states $\{|e_0\rangle, |e_1\rangle\}$ satisfying:

$$(|e_i\rangle, |e_j\rangle) = \delta_{ij}, \quad |e_0\rangle\langle e_0| + |e_1\rangle\langle e_1| = I \tag{28}$$

The interaction Hamiltonian during the identity gate period is:

3.8.2. Decoherence Calculation. For the algorithm $HIH|0\rangle|e_0\rangle$, after the first Hadamard and environmental coupling:

$$|\psi\rangle = \frac{1}{2}[(|0\rangle + |1\rangle)|e_0\rangle + (|0\rangle - |1\rangle)|e_1\rangle] \tag{29}$$

The density matrix is:

$$\begin{aligned}\rho = \frac{1}{4}[&(|0\rangle\langle 0| + |0\rangle\langle 1| + |1\rangle\langle 0| + |1\rangle\langle 1|)|e_0\rangle\langle e_0| \\ &+ (|0\rangle\langle 0| - |0\rangle\langle 1| - |1\rangle\langle 0| + |1\rangle\langle 1|)|e_1\rangle\langle e_1| \\ &+ \text{cross terms}]\end{aligned} \tag{30}$$

Tracing out the environment:

$$\rho_{\text{sys}} = \text{Tr}_{\text{env}}(\rho) = \frac{1}{2}(|0\rangle\langle 0| + |1\rangle\langle 1|) \tag{31}$$

This is a completely mixed state - all coherence between $|0\rangle$ and $|1\rangle$ is lost.The resultant qubit behaves like classical qubit. The final Hadamard gate cannot restore the original state, resulting in:

$$P(|0\rangle) = P(|1\rangle) = 0.5 \tag{32}$$

3.9. Additional Error Channels in Quantum Systems

Quantum information processing platforms exhibit diverse error mechanisms beyond standard decoherence, each requiring specialized mathematical treatment and platform-specific correction strategies.

3.9.1. Measurement Imperfections. In superconducting transmon qubits, measurement errors arise from resonator-induced dephasing and finite measurement fidelity. The measurement process can be modeled using non-ideal POVM elements:

$$\begin{aligned}F_0 &= (1-p_m)|0\rangle\langle 0| + p_m|1\rangle\langle 1|, \\ F_1 &= (1-p_m)|1\rangle\langle 1| + p_m|0\rangle\langle 0|,\end{aligned} \tag{33}$$

where p_m represent probability of error.

3.9.2. Qubit Loss Processes. In semiconductor quantum dot arrays, qubit loss occurs through charge noise-induced tunneling:

$$\rho \to \mathcal{K}_0\rho\mathcal{K}_0^\dagger + \mathcal{K}_1\rho\mathcal{K}_1^\dagger, \tag{34}$$

with Kraus operators:

$$\begin{aligned}\mathcal{K}_0 &= |\text{vac}\rangle\langle 0| + |\text{vac}\rangle\langle 1|, \\ \mathcal{K}_1 &= \sqrt{1-\gamma}(|0\rangle\langle 0| + |1\rangle\langle 1|),\end{aligned} \tag{35}$$

where $|\text{vac}\rangle$ represents the vacuum state and γ denotes the loss probability.

The comprehensive characterization of these diverse error mechanisms reveals that successful fault-tolerant quantum computation requires co-design of quantum hardware with error correction protocols. Each physical platform exhibits unique dominant error channels, necessitating tailored approaches including asymmetric error models for measurement imperfections, loss-tolerant encodings for quantum dot systems, purification protocols for initialization errors, and leakage reduction operations for multi-level quantum systems. This platform-specific understanding enables the development of robust quantum error correction strategies that address the particular challenges of each hardware implementation, ultimately paving the way for scalable fault-tolerant quantum computation.

4. The 3-Qubit Bit-Flip Code

4.1. Code Definition and Encoding

The 3-qubit repetition code, introduced by Shor [2], encodes a single logical qubit into three physical qubits with protection against single bit-flip (X) errors. The logical basis states are:

$$|0\rangle_L = |000\rangle, \quad |1\rangle_L = |111\rangle \tag{36}$$

An arbitrary logical state $|\psi\rangle = \alpha|0\rangle + \beta|1\rangle$ maps to:

$$|\psi\rangle_L = \alpha|000\rangle + \beta|111\rangle \tag{37}$$

4.2. Code Distance and Error Correction Capability

The code distance d is the minimum Hamming distance between codewords:

$$d = \min_{i\neq j} d_H(|i\rangle_L, |j\rangle_L) = 3 \tag{38}$$

This enables correction of $t = \lfloor (d-1)/2 \rfloor = 1$ bit-flip error.

4.3. Encoding Circuit

The encoding unitary is:

$$U_{\text{enc}} = \text{CNOT}_{1,3} \cdot \text{CNOT}_{1,2} \tag{39}$$

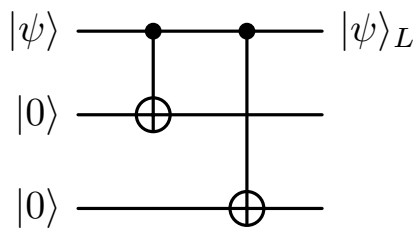

Figure 3: Quantum circuit to prepare the logical state $|\psi\rangle_L$.

4.4. Error Detection and Syndrome Measurement

Error correction proceeds by measuring two parity-check operators without collapsing the encoded state. Two ancilla qubits extract syndrome information:

Syndrome 1: Parity of qubits 1 and 2 **Syndrome 2:** Parity of qubits 2 and 3

TABLE 1: Syndrome Table for 3-Qubit Code

Syndrome (s_1, s_2)	Error Location	Correction
(0, 0)	No error	None
(1, 1)	Qubit 1	X_1
(1, 0)	Qubit 2	X_2
(0, 1)	Qubit 3	X_3

In this experiment, we perform a Monte Carlo simulation of the three-qubit bit-flip quantum error correction code (QECC) using Qiskit to evaluate its ability to preserve the logical qubit state under random single-qubit errors. The logical qubit is initialized as $|\psi\rangle = \alpha|0\rangle + \beta|1\rangle$ with $\alpha = \sqrt{0.7}$ and $\beta = \sqrt{0.3}$, corresponding to ideal measurement probabilities of $|\alpha|^2 = 0.7$ and $|\beta|^2 = 0.3$. The encoding step maps this logical qubit into three physical qubits using two CNOT operations to create redundancy, followed by the injection of a random bit-flip error (X) on one of the three qubits in each trial. Error syndromes are extracted using two ancilla qubits through parity checks, allowing conditional correction based on the measured syndrome pattern. After decoding and measurement, this process is repeated across multiple trials (Monte Carlo runs), and the observed average output probabilities are compared with the theoretical expectations. The results demonstrate that, on average, the observed probabilities closely match the ideal values, confirming that the bit-flip code effectively restores the logical qubit and maintains high fidelity even under random error occurrences.

4.5. Mathematical Analysis of Error Suppression

Consider a coherent rotation error $U_E = e^{i\epsilon X}$ with $\epsilon \ll 1$ acting on all qubits:

$$E = U_E^{\otimes 3} = (c_0 I + c_1 X)^{\otimes 3} \tag{40}$$

where $c_0 = \cos(\epsilon)$, $c_1 = i\sin(\epsilon)$.

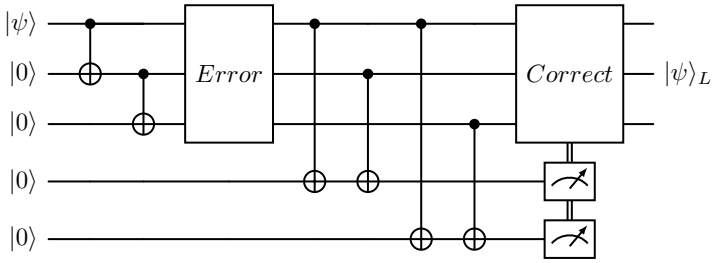

Figure 4: Error Correction Circuit for Bit-Flip

Expanding:

$$E\,|\psi\rangle_L = c_0^3\,|\psi\rangle_L + c_1^3 X_1X_2X_3\,|\psi\rangle_L \tag{41}$$
$$+ c_0^2c_1(X_1 + X_2 + X_3)\,|\psi\rangle_L$$
$$+ c_0c_1^2(X_1X_2 + X_2X_3 + X_1X_3)\,|\psi\rangle_L \tag{42}$$

After syndrome measurement and correction(U_{QEC} is the corresponding operator):

$$\begin{aligned} U_{\text{QEC}}\big(E|\psi\rangle_L|00\rangle\big) = {} & c_0^3|\psi\rangle_L|00\rangle \\ & + c_0^2c_1\sigma_x\sigma_I\sigma_I|\psi\rangle_L|11\rangle \\ & + c_0^2c_1\sigma_I\sigma_x\sigma_I|\psi\rangle_L|10\rangle \\ & + c_0^2c_1\sigma_I\sigma_I\sigma_x|\psi\rangle_L|01\rangle \\ & + c_0c_1^2\sigma_x\sigma_x\sigma_I|\psi\rangle_L|01\rangle \\ & + c_0c_1^2\sigma_I\sigma_x\sigma_x|\psi\rangle_L|11\rangle \\ & + c_0c_1^2\sigma_x\sigma_I\sigma_x|\psi\rangle_L|10\rangle \\ & + c_1^3\sigma_x\sigma_x\sigma_x|\psi\rangle_L|00\rangle \end{aligned} \tag{43}$$

Ancilla Measurement	Collapsed State (with correction)
00	$c_0\|\psi\rangle_L + c_3\sigma_x\sigma_x\sigma_x\|\psi\rangle_L$
01	$c_1\|\psi\rangle_L + c_2\sigma_x\sigma_x\sigma_x\|\psi\rangle_L$
10	$c_1\|\psi\rangle_L + c_2\sigma_x\sigma_x\sigma_x\|\psi\rangle_L$
11	$c_1\|\psi\rangle_L + c_2\sigma_x\sigma_x\sigma_x\|\psi\rangle_L$

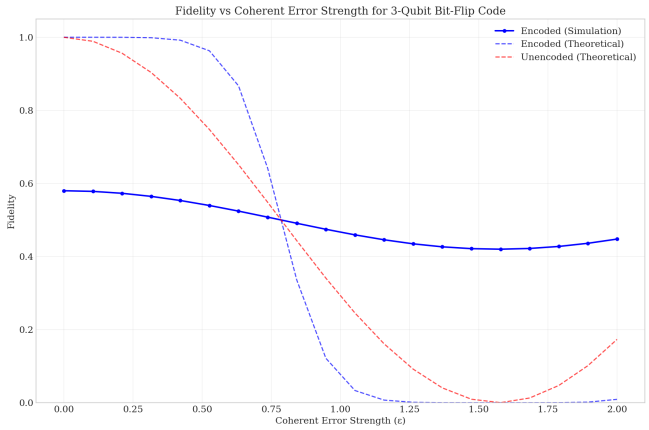

Figure 5: Fidelity comparision

The encoded qubit error rate is suppressed from $O(\epsilon^2)$ to $O(\epsilon^6)$ in the best case, demonstrating the power of redundant encoding. PLot below shows fidelity comparision for simulated and theoretical values.This shows that shor's code works well for high epsilon values as well. The unencoded scheme while only outperforms shor's code at low epsilon values.

5. 3-Qubit Phase flip Code

The phase flip error correction circuit was implemented using Qiskit through a structured six-phase protocol. The implementation begins with register initialization, allocating three data qubits for state encoding and two ancilla qubits for syndrome measurement. State encoding employs Hadamard gates to transform phase errors into detectable bit-flip errors within the conjugate basis, followed by controlled error injection where random σ_z errors are introduced on individual data qubits.

Syndrome measurement constitutes the core error detection mechanism, utilizing parity checks between specific qubit pairs. The first syndrome measurement assesses parity between qubits 0 and 2 via ancilla[0], while the second syndrome evaluates parity between qubits 1 and 2 through ancilla[1]. These measurements generate unique binary signatures that precisely identify error locations according to the established syndrome mapping protocol.

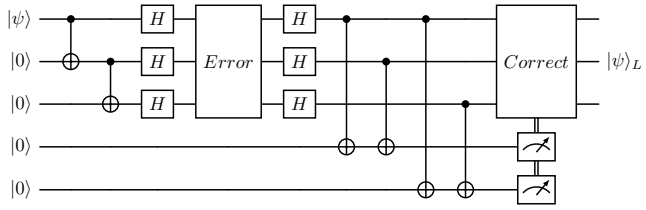

Figure 6: Error Correction Circuit for Phase Flip

Syndrome (s_1, s_2)	**Error Location**	**Correction**
(0,0)	No error	None
(0,1)	Qubit 0	Z_2
(1,0)	Qubit 1	Z_1
(1,1)	Qubit 2	Z_0

TABLE 2: Syndrome mapping for phase flip error correction. The syndrome bits s_1 and s_2 represent parity measurements between qubit pairs (0,2) and (1,2) respectively.

6. The 9-Qubit Shor Code

6.1. Limitations of the 3-Qubit Code

The 3-qubit code only protects against bit-flip errors. Phase errors Z anticommute with the logical $\overline{X}$ operator:

$$Z_i(\alpha\,|000\rangle + \beta\,|111\rangle) = \alpha\,|000\rangle \pm \beta\,|111\rangle \tag{44}$$

which cannot be detected by X-parity checks.

6.2. Shor Code Construction

Shor's 9-qubit code [2] provides simultaneous protection against single X and/or Z errors through concatenated encoding. The logical basis states are:

$$|0\rangle_L = \frac{1}{2\sqrt{2}}(|000\rangle + |111\rangle)^{\otimes 3}$$
$$|1\rangle_L = \frac{1}{2\sqrt{2}}(|000\rangle - |111\rangle)^{\otimes 3} \tag{45}$$

6.3. Error Correction Structure

The code is a degenerate code where different physical errors can have the same effect on logical states. The 9 qubits are divided into three blocks of three qubits each.

Bit-flip correction: Within each block, apply the 3-qubit repetition code correction circuit.

Phase-flip correction: Measure the relative phase between blocks using 6 CNOT gates:

- Compare blocks 1 and 2
- Compare blocks 2 and 3

6.4. Syndrome Measurement

X-error syndromes: Three sets of two-bit syndromes, one for each block.

Z-error syndromes: Two-bit syndrome comparing block phases:

$$s_1 = \text{parity}(\text{block}_1, \text{block}_2) \tag{46}$$
$$s_2 = \text{parity}(\text{block}_2, \text{block}_3) \tag{47}$$

TABLE 3: Z-Error Syndrome Table

Syndrome (s_1, s_2)	Error Block	Correction
(0, 0)	No phase error	None
(1, 1)	Block 1	Z on any qubit in block 1
(1, 0)	Block 2	Z on any qubit in block 2
(0, 1)	Block 3	Z on any qubit in block 3

6.5. Degeneracy and Correction

The code exhibits degeneracy: different physical errors map to the same logical error. For example, any single Z error within a block produces the same syndrome, so correction can apply Z to any qubit in that block.

For a simultaneous bit and phase error on the same qubit:

$$Y_i = iX_iZ_i \tag{48}$$

The X correction circuit handles the bit-flip component, while the Z correction circuit handles the phase-flip, effectively correcting the Y error.

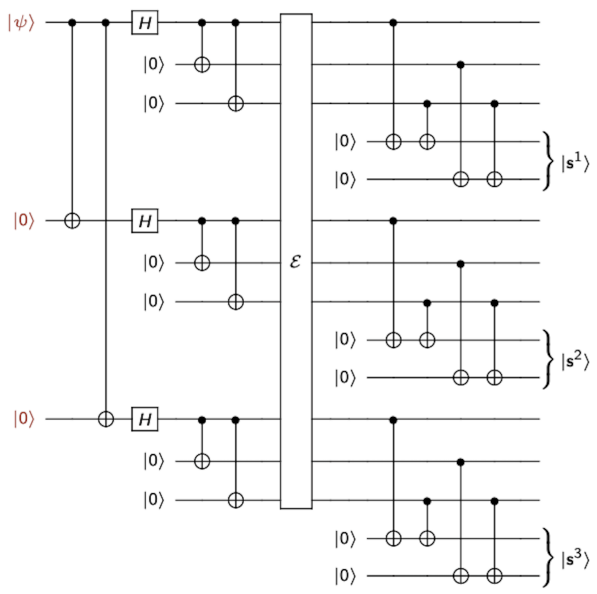

Figure 7: Encoding and error correction structure of the 9-qubit Shor code. The circuit shows the concatenated repetition encoding for bit-flip and phase-flip protection.

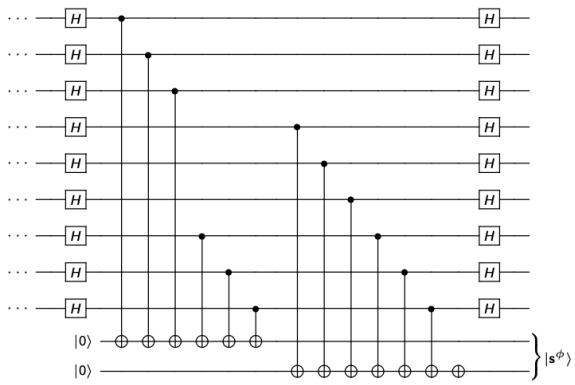

Figure 8: Phase error detection and syndrome measurement in the Shor code. The circuit compares relative phases between the three blocks.

6.6. Code Parameters

The Shor code is a $[[9, 1, 3]]$ quantum code with:

- $n = 9$ physical qubits
- $k = 1$ logical qubit encoded
- $d = 3$ minimum distance
- Corrects any single Pauli error (X, Y, or Z)

7. Quantum Error Detection

7.1. Detection vs Correction

Error detection requires fewer resources than error correction but provides less powerful error suppression. Detection schemes identify that an error occurred without necessarily determining its location, allowing rejection of corrupted states in post-selected protocols [6].

7.2. The 4-Qubit Error Detection Code

The 4-qubit code encodes two logical qubits into four physical qubits with single error detection capability. The four logical basis states are:

$$|00\rangle_L = \frac{1}{\sqrt{2}}(|0000\rangle + |1111\rangle) \tag{49}$$

$$|01\rangle_L = \frac{1}{\sqrt{2}}(|1100\rangle + |0011\rangle) \tag{50}$$

$$|10\rangle_L = \frac{1}{\sqrt{2}}(|1010\rangle + |0101\rangle) \tag{51}$$

$$|11\rangle_L = \frac{1}{\sqrt{2}}(|0110\rangle + |1001\rangle) \tag{52}$$

7.3. Detection Circuit and Syndrome

Two ancilla qubits measure global parity properties:

$$s_1 = \text{parity of all 4 qubits (X-type)} \tag{53}$$

$$s_2 = \text{parity of all 4 qubits (Z-type)} \tag{54}$$

For any single X or Z error, at least one syndrome returns $|1\rangle$, indicating error detection. However, the syndrome does not reveal the error location, only that an error occurred.

7.4. Post-Selection Protocol

In post-selected quantum computation:

1) Prepare many encoded ancilla states
2) Apply error detection
3) Accept only states with syndrome $(0, 0)$
4) Use accepted states for further computation

The detection approach enables higher error thresholds in some architectures at the cost of probabilistic acceptance rates.

8. Stabilizer Formalism

8.1. Motivation and Heisenberg Representation

The stabilizer formalism, introduced by Gottesman [5], provides a powerful algebraic framework for quantum error correction. Instead of specifying quantum states by their wavefunction amplitudes, states are characterized by the set of operators that leave them invariant.

8.2. Mathematical Foundation

A quantum state $|\psi\rangle$ is stabilized by an operator K if it is a $+1$ eigenstate:

$$K|\psi\rangle = |\psi\rangle \tag{55}$$

For example, $|0\rangle$ is stabilized by Z since $Z|0\rangle = |0\rangle$, while $|1\rangle$ satisfies $Z|1\rangle = -|1\rangle$.

8.3. The n-Qubit Pauli Group

The n-qubit Pauli group is defined as:

$$\mathcal{P}_n = \{\pm 1, \pm i\}^{\otimes n} \times \{I, X, Y, Z\}^{\otimes n} \tag{56}$$

Key properties:

- Group size: $|\mathcal{P}_n| = 4^{n+1}$
- All elements square to $\pm I$
- Any two elements either commute or anticommute

8.4. Stabilizer States and Groups

An n-qubit stabilizer state $|\psi\rangle$ is uniquely defined by n independent stabilizer generators $\{K_1, K_2, \ldots, K_n\}$ that:

1) Commute pairwise: $[K_i, K_j] = 0$ for all i, j
2) Stabilize the state: $K_i|\psi\rangle = |\psi\rangle$ for all i
3) Are independent: no K_i equals $\prod_{j\neq i} K_j^{a_j}$

The stabilizer group is:

$$\mathcal{S} = \langle K_1, K_2, \ldots, K_n\rangle = \left\{\prod_{i=1}^{n} K_i^{a_i} : a_i \in \{0,1\}\right\} \tag{57}$$

8.5. Important Stabilizer States

8.5.1. Bell States. The four Bell states are characterized by:

$$|\Phi^+\rangle = \frac{1}{\sqrt{2}}(|00\rangle + |11\rangle): \quad K_1 = XX, \quad K_2 = ZZ \tag{58}$$

$$|\Phi^-\rangle = \frac{1}{\sqrt{2}}(|00\rangle - |11\rangle): \quad K_1 = -XX, \quad K_2 = ZZ \tag{59}$$

$$|\Psi^+\rangle = \frac{1}{\sqrt{2}}(|01\rangle + |10\rangle): \quad K_1 = XX, \quad K_2 = -ZZ \tag{60}$$

$$|\Psi^-\rangle = \frac{1}{\sqrt{2}}(|01\rangle - |10\rangle): \quad K_1 = -XX, \quad K_2 = -ZZ \tag{61}$$

8.6. Hilbert Space Decomposition

For an n-qubit system with k independent stabilizer generators, the stabilized subspace has dimension:

$$\dim(\mathcal{H}_{\text{stab}}) = 2^{n-k} \tag{62}$$

This enables encoding of $n-k$ logical qubits into n physical qubits.

9. QEC with Stabilizer Codes

9.1. Code Space Definition

A stabilizer quantum error correcting code $\mathcal{C}$ encoding k logical qubits into n physical qubits is defined by $n-k$ stabilizer generators:

$$\mathcal{C} = \{|\psi\rangle \in \mathcal{H}^{\otimes n} : K_i|\psi\rangle = |\psi\rangle,\ i = 1, \ldots, n-k\} \tag{63}$$

The code is denoted $[[n, k, d]]$ where d is the minimum distance.

9.2. Logical Operators

Logical Pauli operators $\overline{X}_j, \overline{Z}_j$ for the j-th logical qubit satisfy:

- Commute with all stabilizers: $[\overline{X}_j, K_i] = [\overline{Z}_j, K_i] = 0$
- Act nontrivially on code space: $\overline{X}_j|0\rangle_L^{(j)} = |1\rangle_L^{(j)}$
- Anticommute between X and Z: $\{\overline{X}_j, \overline{Z}_j\} = 0$

9.3. Steane [[7,1,3]] Code

The 7-qubit Steane code is the most well-known CSS (Calderbank-Shor-Steane) code, with logical states:

$$|0\rangle_L = \frac{1}{2\sqrt{2}} \sum_{w\in C_7} |w\rangle \tag{64}$$

$$|1\rangle_L = \frac{1}{2\sqrt{2}} \sum_{w\in C_7} (-1)^{|w|}|w\rangle \tag{65}$$

where C_7 is the classical $[7, 4, 3]$ Hamming code.

9.3.1. Stabilizer Generators. The six stabilizers separate into X-type and Z-type:

$$K_1 = IIIXXXX \tag{66}$$
$$K_2 = IXXIIXX \tag{67}$$
$$K_3 = XIXIXIX \tag{68}$$
$$K_4 = IIIZZZZ \tag{69}$$
$$K_5 = IZZIIZZ \tag{70}$$
$$K_6 = ZIZIZIZ \tag{71}$$

9.3.2. Logical Operators.

$$\overline{X} = XXXXXXX \tag{72}$$
$$\overline{Z} = ZZZZZZZ \tag{73}$$

Each stabilizer has weight 4 (four non-identity operators), ensuring $[\overline{X}, K_i] = [\overline{Z}, K_i] = 0$ since each picks up two anticommutations.

9.4. State Preparation via Stabilizer Measurement

9.4.1. Eigenstate Projection. To prepare a state stabilized by operator K, we measure K on an arbitrary input. The measurement projects to:

$$|\psi'\rangle \propto (I + K)\,|\psi\rangle \tag{74}$$

if outcome is $+1$, or:

$$|\psi'\rangle \propto (I - K)\,|\psi\rangle \tag{75}$$

if outcome is -1.

9.4.2. Steane Code Preparation. Starting from $|0\rangle^{\otimes 7}$:

1) Measure K_1, K_2, K_3 (X-type stabilizers)
2) Apply single-qubit Z corrections based on outcomes to ensure $+1$ eigenvalues
3) No need to measure K_4, K_5, K_6 since $|0\rangle^{\otimes 7}$ is already in their $+1$ eigenspace

The circuit implements:

$$|0\rangle_L = \prod_{i=1}^{3} P_i^+ \,|0\rangle^{\otimes 7} \tag{76}$$

where $P_i^+ = (I + K_i)/2$ projects to $+1$ eigenspace.

9.5. Error Detection and Correction

9.5.1. Error Syndrome. An error $E \in \mathcal{P}_n$ (which anti-commutes with K_i operator) acting on a code state $|\psi\rangle_L$ produces:

$$E\,|\psi\rangle_L \tag{77}$$

Measuring stabilizer K_i yields:

$$s_i = \begin{cases} +1 & \text{if } [E, K_i] = 0 \\ -1 & \text{if } \{E, K_i\} = 0 \end{cases} \tag{78}$$

The syndrome vector $\mathbf{s} = (s_1, s_2, \ldots, s_{n-k})$ uniquely identifies correctable errors.

9.5.2. Correction Protocol.

1) Measure all stabilizers: $K_1, K_2, \ldots, K_{n-k}$
2) Compute syndrome: $\mathbf{s} = (s_1, \ldots, s_{n-k})$
3) Look up error $\hat{E}$ in syndrome table
4) Apply correction: $\hat{E}^\dagger E\,|\psi\rangle_L$

If $\hat{E}^\dagger E$ commutes with all stabilizers and logical operators, correction succeeds.

Future Work and Conclusion

In future work, we aim to complete our review of the remaining literature, focusing on the **digitization of quantum errors**, the **Fault-Tolerant Quantum Error Correction and Threshold Theorem**, and **fault-tolerant circuit design for logical state preparation**. We will also examine recent advances discussed in **modern developments in quantum error correction**. These studies will help us build a stronger foundation for understanding and simulating fault-tolerant quantum systems, ultimately guiding future implementation and optimization efforts.

References

[1] S. J. Devitt, W. J. Munro, and K. Nemoto, "Quantum error correction for beginners," *Reports on Progress in Physics*, vol. 76, no. 7, p. 076001, 2013.

[2] P. W. Shor, "Scheme for reducing decoherence in quantum computer memory," *Physical Review A*, vol. 52, no. 4, p. R2493, 1995.

[3] A. M. Steane, "Error correcting codes in quantum theory," *Physical Review Letters*, vol. 77, no. 5, p. 793, 1996.

[4] D. Aharonov and M. Ben-Or, "Fault-tolerant quantum computation with constant error rate," in *Proceedings of the 29th Annual ACM Symposium on Theory of Computing*, 1997, pp. 176–188.

[5] D. Gottesman, "Stabilizer codes and quantum error correction," Ph.D. dissertation, California Institute of Technology, 1997.

[6] E. Knill, "Quantum computing with realistically noisy devices," *Nature*, vol. 434, no. 7029, pp. 39–44, 2005.

[7] M. A. Nielsen and I. L. Chuang, *Quantum Computation and Quantum Information*, 10th ed. Cambridge University Press, 2010.

[8] W. K. Wootters and W. H. Zurek, "A single quantum cannot be cloned," *Nature*, vol. 299, no. 5886, pp. 802–803, 1982.

[9] J. Preskill, "Quantum computing in the NISQ era and beyond," *Quantum*, vol. 2, p. 79, 2018.